Effect of Span and MRD Configurations on Small Animal PET Image Quality and Quantitative Accuracy

Tahereh Zare (PhD)[1,2], Mohammad Ghorbanzadeh (MSc)[2], Behnoosh Teimourian Fard (PhD)[2], Peyman Sheikhzadeh (PhD)[1,3], Pardis Ghafarian (PhD)[4,5], Sanaz Hariri Tabrizi (PhD)[2], Mohammad Hossein Farahani (MSc)[2], Mohammad Reza Ay (PhD)[1,2]*

[1]Department of Medical Physics and Biomedical Engineering, Tehran University of Medical Sciences, Tehran, Iran
[2]Research Center for Molecular and Cellular Imaging (RCMCI), Advanced Medical Technologies and Equipment (AMTEI), Tehran University of Medical Sciences (TUMS), Tehran, Iran
[3]Department of Nuclear Medicine, Imam Khomeini Hospital Complex, Tehran University of Medical Sciences, Tehran, Iran
[4]Chronic Respiratory Diseases Research Center, National Research Institute of Tuberculosis and Lung Diseases (NRITLD), Shahid Beheshti University of Medical Sciences, Tehran, Iran
[5]PET/CT and Cyclotron Center, Masih Daneshvari Hospital, Shahid Beheshti University of Medical Sciences, Tehran, Iran

ABSTRACT

Background: Employing 2D rebinned sinograms in PET scanners has the potential to accelerate the overall reconstruction speed. Among the available rebinning techniques, Single-Slice Rebinning (SSRB) offers a computationally efficient approach.

Objective: This study aimed to evaluate the influence of varying span and Maximum Ring Difference (MRD) parameters in SSRB on the image quality of the Xtrim PET scanner.

Material and Methods: This Monte Carlo simulation study used a GATE-simulated Xtrim-PET scanner. 3D list-mode data were histogrammed into 576 sinograms, and SSRB was applied to generate 2D sinograms. Subsequently, Maximum-Likelihood Expectation-Maximization (MLEM) reconstruction was performed on the sinograms with different MRD and span. Image quality was assessed using image quality, rod, and uniform phantoms. Furthermore, axial resolution was evaluated using point sources.

Results: Analysis of linear profiles in uniform phantom revealed a 2.6 mm inaccuracy in axial activity estimation when comparing spans of 21 and 7. Increased span and MRD lead to artifactual data in regions of high activity gradients, as observed in both uniform and rod phantoms. However, the Recovery Coefficient (RC) and Spilled-Over Ratio (SOR) remained unaffected. Concomitantly, increasing the span improved uniformity and reduced the coefficient of variation by 1.6% and 5.9%, respectively. Axial resolution remained largely unaffected by variations in span and MRD.

Conclusion: The RC and SOR remain robust to variations in span and MRD. However, higher levels of axial data compression were associated with the introduction of axial artifacts. Additionally, axial resolution was unaffected by increases in span and MRD, likely due to the limited field of view of the Xtrim-PET scanner.

Citation: Zare T, Ghorbanzadeh M, Teimourian Fard B, Sheikhzadeh P, Ghafarian P, Hariri Tabrizi S, Farahani MH, Ay MR. Effect of Span and MRD Configurations on Small Animal PET Image Quality and Quantitative Accuracy. *J Biomed Phys Eng*. 2025;15(4):323-332. doi: 10.31661/jbpe.v0i0.2502-1893.

Keyword

Positron-Emission Tomography; Image Enhancement, Signal to-Noise Ratio; Rebinning; SSRB

Introduction

Preclinical Positron Emission Tomography (PET) imaging is a nuclear medicine functional imaging modality for studying the disease process over time, biological research [1], and the screening of novel diagnostic/theragnostic PET probes [2]. Methodological

*Corresponding author:
Mohammad Reza Ay
Department of Medical Physics and Biomedical Engineering, Tehran University of Medical Sciences, Tehran, Iran
E-mail: mohammadreza_ay@tums.ac.ir

Received: 15 February 2025
Accepted: 3 March 2025

parameters, including image acquisition, substantially affect PET scanner performance [3].

3D PET data acquisition offers superior data acquisition. However, it comes with significantly higher computational and storage demands [4]. To accelerate the reconstruction process, a hybrid approach was implemented [5]. This method (Hybrid approach) involved first generating a 3D sinogram from the 3D acquisition data to optimize the Signal-to-Noise Ratio (SNR) by reducing noise. To minimize computational time, the 3D sinogram is subsequently rebinned into a sequence of 2D sinograms through techniques, such as Single-Slice Rebinning (SSRB) [6], Multi-Slice Rebinning (MSRB) [7], and Fourier Rebinning (FORE) [8]. Following these rebinning processes, the resulting 2D sinogram is reconstructed utilizing a 2D iterative algorithm, such as Ordered Subset Expectation Maximization (OSEM) or Maximum-Likelihood Expectation-Maximization (MLEM) [9]. The reconstructed 2D slices were then stacked together to produce the final 3D image [8].

The further reduction of data volume in rebinning algorithms is characterized by two key parameters: axial compression (span) factor and Maximum Ring Difference (MRD) [10]. Axial Line Of Response (LOR) combination (sum of odd and even planes) is controlled by the span parameter [11, 12], and MRD restricts the maximum allowable absolute difference in coincidence detection [13].

Rebinning algorithms have the potential to impact the quality of PET images. For example, the research conducted by López-Montes et al. [14] focused on evaluating the influence of different rebinning algorithms, namely SSRB, FORE, and Pseudo-Inverted (PINV), in preclinical PET/CT scanners. The methods yielded comparable uniformity, although recovery coefficients did not show significant improvement. Hasegawa et al. studied how changing the span affected axial resolution on the EXCAT HR+ scanner. They found that axial resolution remained unchanged at the scanner's center, but worsened as the source moved further from the center with wider spans [13].

SSRB as a fast, simplest, and computationally efficient rebinning algorithm is used in preclinical PET scanners [14-18]. Rebinning methods are known to significantly influence the quantification of PET images. Therefore, this research aims to determine the effects of different MRD and span parameters used in SSRB on the quantitative accuracy achieved with the Xtrim-PET scanner. The Xtrim-PET scanner is a commercially available preclinical PET system specifically designed for small animal imaging [19, 20]. This study utilizes image quality phantom, rod phantom, and uniform phantom to evaluate the impact of different SSRB configurations on image quality.

Material and Methods

GATE simulation

1. Xtrim-PET scanner geometry

The Monte Carlo simulation study of the Xtrim-PET scanner was conducted using the GATE (Geant4 Application for Tomographic Emission) software (V9.1). GATE is an open-source Monte Carlo simulation platform used extensively in medical imaging research [21]. Its user-friendly interface facilitates the simulation of realistic models of PET [22, 23] and Single Photon Emission Computed Tomography (SPECT) [24], systems.

This study employed an experimentally validated GATE Monte Carlo simulation model of the Xtrim-PET scanner [25]. The Xtrim-PET consists of 10 detector blocks, arranged in a polygonal full-ring structure with a ring diameter of 162.6 mm. Each block contains a 24×24 array of Lutetium Yttrium Oxyorthosilicate (LYSO) crystals (2×2×10 mm^3) coupled with SiPMs. In both the axial and trans-axial directions, the crystal pixel pitch is 2.1 mm. The trans-axial and axial Field Of View (FOV) are 100 mm and 50 mm, respectively. The energy window was established at 350 to

650 keV, and the coincidence timing window was set to 10 ns. Simulations employed a 17% energy resolution at 511 keV and incorporated a 500 ns dead time at the block level.

2. Phantoms

Rod phantom for count efficiency evaluation: To assess the impact of MRD and span on True Count Efficiency (TCE) (Equation 1), a 1.2 mm diameter × 70 mm height cylindrical rod phantom, containing 1.5 MBq of ^{18}F mixed with water, was centrally positioned within the scanner.

$$TCE(\%) = \frac{True\ Counts\ in\ each\ MRD\ \&\ Span}{Total\ Counts} \quad (1)$$

Image quality phantom: To evaluate the effect of different SSRB algorithm configurations on image quality, NEMA NU-4 2008 image quality phantom [26] was simulated, including three main components: 1) two cold chambers (filled with water and air) for calculating the spillover ratio (SOR), 2) a uniform region for uniformity evaluation, and 3) five fillable rods (diameters: 1, 2, 3, 4, and 5 mm) in a cold background to assess the Recovery Coefficient (RC). The phantom was filled with 3.7 MBq of ^{18}F mixed with water.

Uniform phantom: The uniform phantom, with a diameter of 80 mm and height of 25.85 mm, was filled with 3.7 MBq of ^{18}F mixed with water (Figure 1A). The phantom was placed in the middle of the axial FOV and used to evaluate axial distortion and uniformity.

Rod phantom: To evaluate the effects of larger axial compression in the trans-axial plane, one-rod source with a diameter of 1.2 mm and a height of 20 mm was located at the coordinates (0, +40, +12) mm. The rod's longitudinal axis is perpendicular to the scanner's central axis (Figure 1B).

Point sources: Radial and axial spatial resolution were quantified for varying spans and MRDs using six cylindrical sources (1 mm diameter and 1 mm height) containing 1 MBq of ^{18}F aqueous solution. These sources were positioned at 0, 10, and 25 mm radial offsets within the trans-axial FOV, and at a single axial offset representing one-quarter of the axial FOV.

Sinogram rebinning and reconstruction

The list-mode data from the GATE simulation (ASCII output) were stored and subsequently data were histogrammed into 576 sinograms in 3D mode. The implementation of SSRB on a PET scanner equipped with Z detector rings involves mapping a coincidence event occurring between rings Z_1 and Z_2 to the rebinned sinogram plane at the coordinate $(Z_1+Z_2)/2$ (Figure 2). Therefore, the SSRB algorithm, which assigns oblique LORs to the middle axial slice (4), was applied to create 2D sinograms with 240 radial bins and 310 angular bins.

These 2D SSRB sinograms were generated with different combinations of MRD and span. The selection of the span and MRD for each combination is made to ensure that only a single segment is present in the rebinned sinogram. The SSRB-rebinned sinograms (using true and scatter coincidences) were then reconstructed using the attenuation-weighted MLEM (AW-MLEM) algorithm (20 iterations

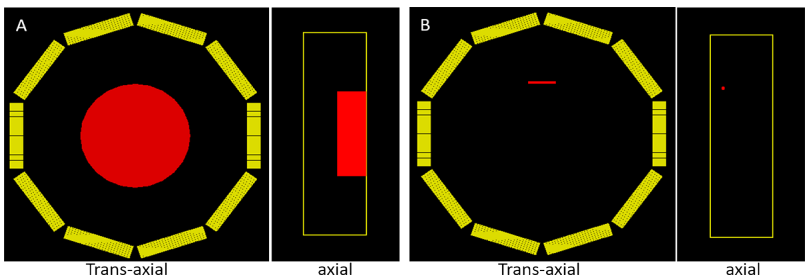

Figure 1: Trans-axial and axial view of **A**) Uniform Phantom, and **B**) rod source within the Xtrim- Positron Emission Tomography (PET) scanner geometry.

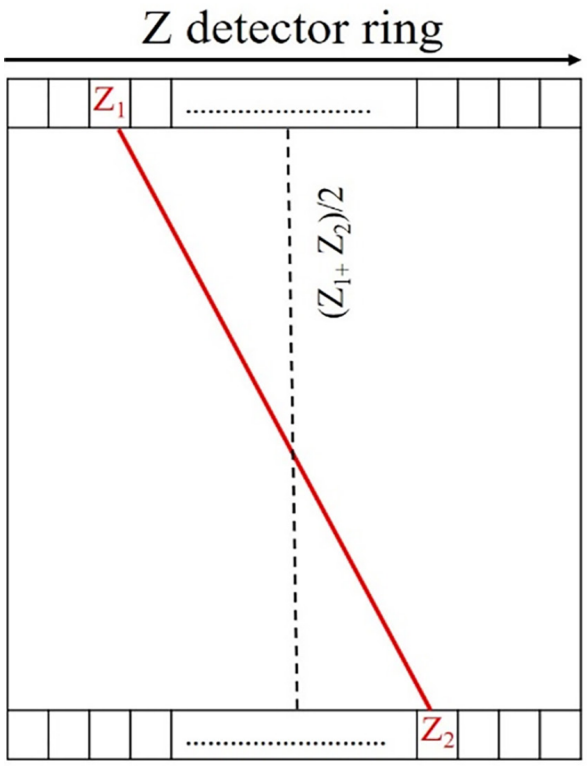

Figure 2: Schematic representation of Single-Slice Rebinning (SSRB) algorithm for a scanner with Z detector ring.

and voxel size of 0.5×0.5×1.05 mm^3) without scatter correction, utilizing an in-house software. Attenuation correction was performed using Chang's method [27], a non-transmission attenuation correction approach, applied to the uniform regions in PET and SPECT imaging systems.

Assessment strategy

Image analysis was conducted using Amide software (Version 1.0.4) [28]. Image uniformity was evaluated using the Coefficient of Variation (COV) and Integral Uniformity (IU) [29], as described in Equations 2 and 3. The SNR was calculated by taking the ratio of the mean value to the standard deviation of the uniform phantom. The parameters were determined by utilizing a cylindrical Volume Of Interest (VOI) that encompasses 75% of the active diameter, positioned at the center of both the uniform phantom and the uniform region of the image quality phantom.

$$COV = \frac{\text{Standard Deviation in ROI}}{\text{Mean Pixel value in ROI}} \quad (2)$$

$$\text{IU} = \frac{\text{Maximum value in ROI} - \text{minimum value in ROI}}{\text{maximum value in ROI} + \text{minimum valu in ROI}} \quad (3)$$

The RC and SOR in the image quality phantom were calculated based on Equations 4 and 5 with the recommendations provided by the NEMA NU4.

$$RC = \frac{C_h}{C_b} \quad (4)$$

$$SOR = \frac{C_c}{C_b} \quad (5)$$

Where C_h, C_c, and C_b represent the mean counts in the hot, cold, and background (uniform) areas, respectively.

Results

Count efficiency: Analysis of TCE and random count data (Figure 3) across varying MRD and span configurations reveals a positive correlation between TCE and both parameters. A similar trend was observed for random and scattered events, indicating a potential influence on the quality of the reconstructed images.

Uniform phantom: Figure 4 illustrates the positive correlation between image quality metrics and both span and MRD in a uniform phantom. Specifically, higher span and MRD values led to improved IU, a reduced COV, and an enhanced SNR, as expected.

Figure 5A shows the sagittal view of the uniform phantom reconstructed with different MRD and span. As observed, increasing the span and MRD causes the edge of the phantom, located at the center of the axial FOV, to exhibit curvature. To facilitate better analysis, a linear profile is also presented in Figure 5B to facilitate better analysis. As the span and MRD increase, the data assigned to the adjacent slice also increases, evident from the decreasing slope of the line.

The spatial difference between the 80% and

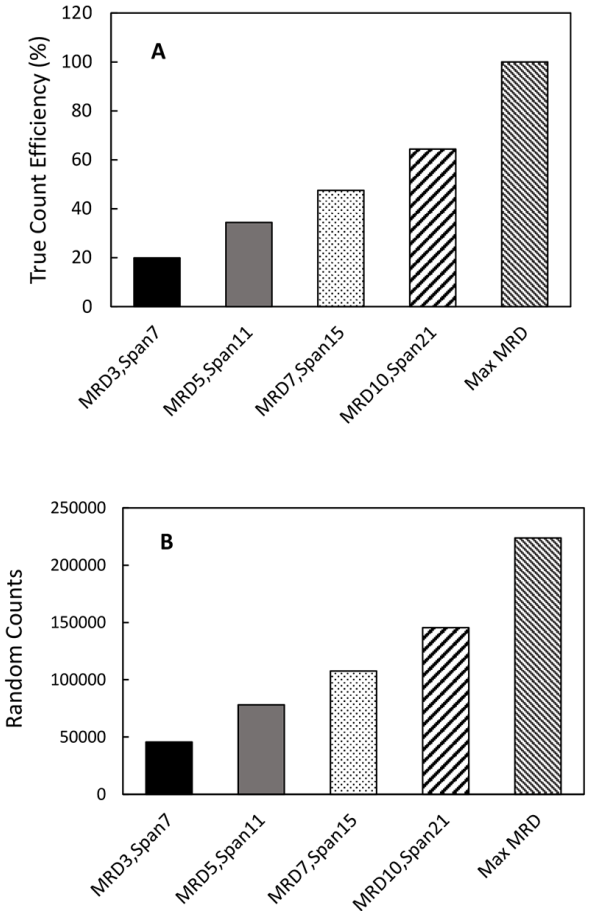

Figure 3: A) True Count Efficiency (TCE) and **B**) random count for each Maximum Ring Difference (MRD) and span

30% peak profile for various MRD and span configurations are as follows: 2.1 mm for MRD=3 and span=7, 3.57 mm for MRD=5 and span=11, 3.15 mm for MRD=7 and span=15, and 4.7 mm for MRD=10 and span=21. These results indicate that increasing the span and MRD can cause distortion in the axial direction, which can also affect the quality of the reconstructed image.

Rod phantom: Figure 6 presents reconstructed images of a rod phantom acquired with different MRD and span. Increased MRD and span demonstrably introduce distortion, manifesting as curvature in the rod. This distortion arises from the incorporation of increasingly oblique sinogram data. The resulting image artifacts can compromise the accuracy of activity quantification, particularly within the FOV periphery.

Image quality phantom: The impact of increased span and MRD on image quality, assessed using an image quality phantom, is summarized in Table 1. Analysis of the uniform region showed that increasing the span and MRD parameters to 11 and 5, respectively, resulted in a 5% enhancement in IU. However, subsequent increments to these parameters produced negligible improvement

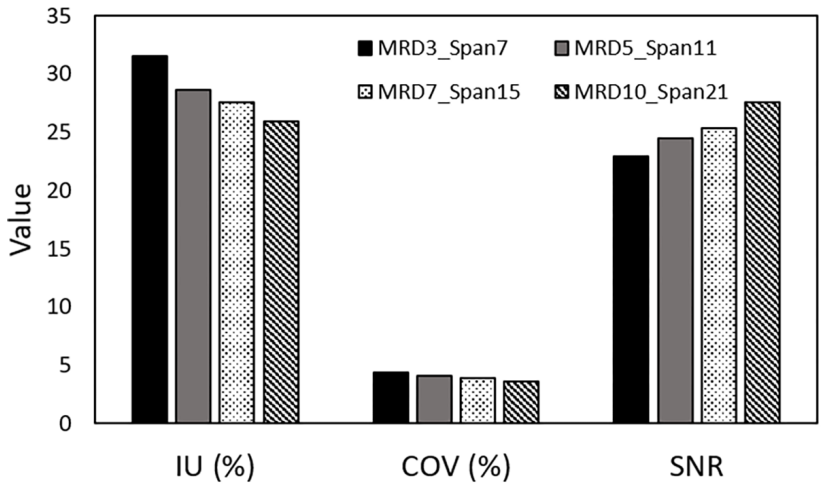

Figure 4: The Integral Uniformity (IU), Coefficient of Variation (COV), and Signal-to-Noise Ratio (SNR) in the uniform phantom for different spans and Maximum Ring Difference (MRD).

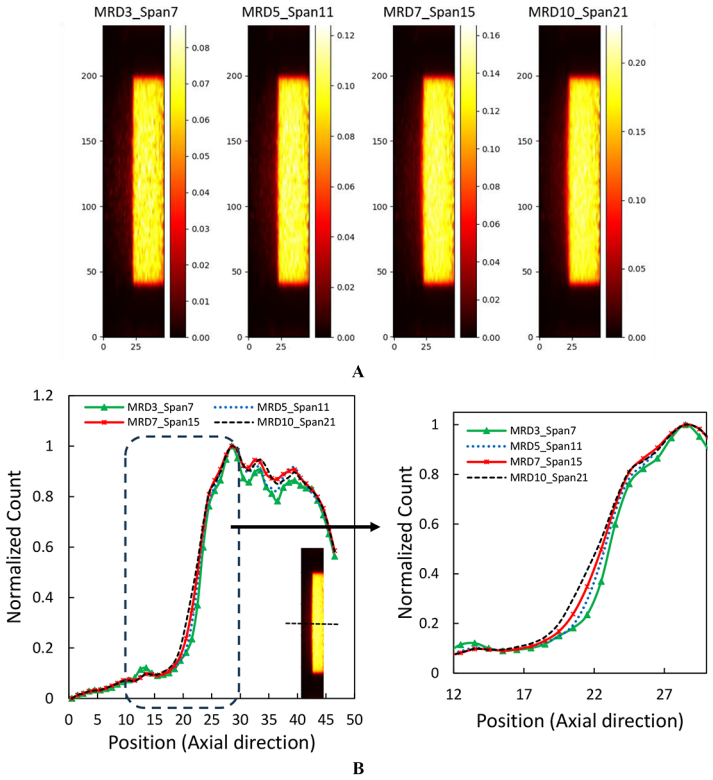

Figure 5: **A**) The sagittal view of the uniform phantom with different Maximum Ring Differences (MRD) and spans and **B**) corresponding intensity line profile.

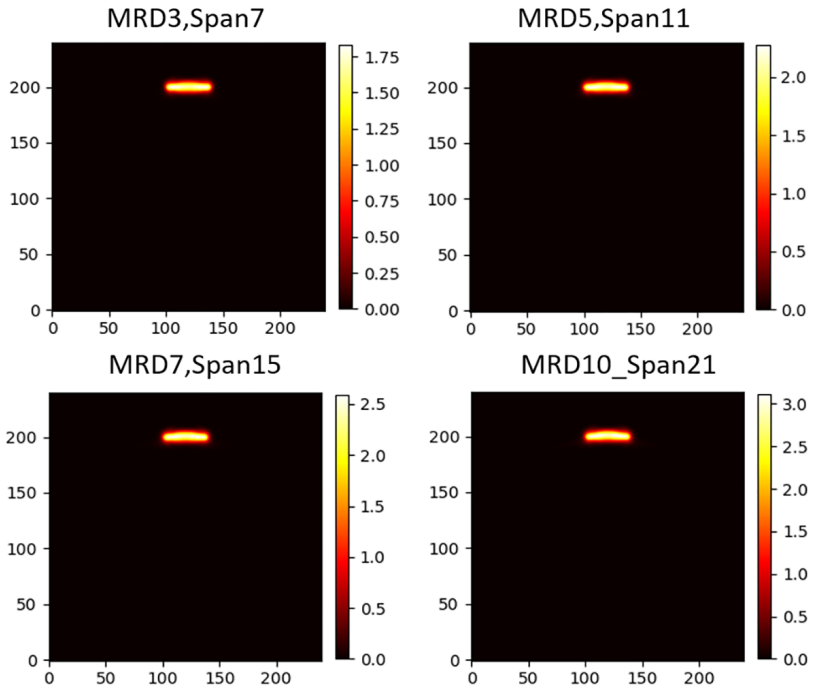

Figure 6: The transverse view of the rod phantom with different Maximum Ring Differences (MRD) and spans.

in uniformity (<1.5%). Also, SOR remained largely unaffected across the water and air cold chambers. Additionally, Figure 7 illustrates that changes in span and MRD had little effect on the RC across different rod diameters. A slight, non-significant reduction in RC was observed only in the 2, 3, and 5 mm diameter rods.

Spatial resolution: The analysis of spatial resolution is illustrated in Table 2. As expected, increasing radial offset resulted in a degradation in both radial and axial resolution, both center and axial off-center. Importantly, neither radial nor axial resolution showed a correlation with changes in span or MRD.

Discussion

This study investigated the effects of varying span and MRD parameters on SSRB algorithm in image quality and quantitative accuracy in the Xtrim-PET scanner. The findings provide valuable insights into the trade-offs between improving SNR and image uniformity, while addressing the challenges posed by axial distortion and activity misassignment at higher span and MRD values.

In all configurations, the ratios of randoms-to-true and scatter-to-true exhibited remarkable consistency, averaging approximately 0.019 and 0.035, respectively. Also, by shorter MRD and span factor, the probability of recording true events decreased. This finding aligns with the previously observed reported by Adam et al., [30]. Utilizing low MRD and span values restricts the amount of data available for reconstruction, leading to a reduction

Table 1: The effect of Maximum Ring Difference (MRD) and span on uniformity and Spilled Over Ratio (SOR) in the image quality phantom. Integral Uniformity (IU) and Coefficient of Variation (COV).

	Uniform Region		Water Chamber	Air Chamber
	IU (%)	COV (%)	SOR (%)	SOR (%)
MRD3, Span7	16.0	4.0	26.3	23.0
MRD5, Span11	11.0	3.2	26.0	23.8
MRD7, Span15	9.6	2.7	26.2	24.1
MRD10, Span21	9.1	2.4	25.7	23.9

MRD: Maximum Ring Difference, IU: Integral Uniformity, COV: Coefficient of Variation, SOR: Spilled Over Ratio

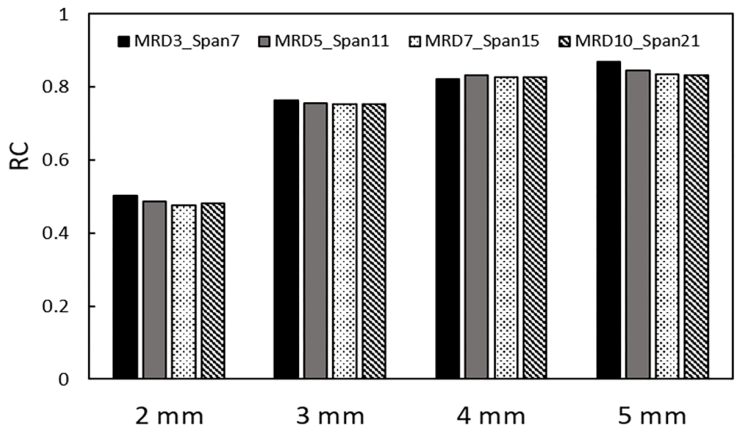

Figure 7: The effect of Maximum Ring Difference (MRD) and Span on Recovery Coefficient (RC) in the image quality phantom.

Table 2: The radial and axial spatial resolution in the center and off-center of Axial Field of View (AFOV) for different Maximum Ring Difference (MRD) and Span configurations.

		Center of AFOV			Off Center in AFOV		
		Radial distance (mm)			Radial distance (mm)		
		0	10	25	0	10	25
Radial Resolution	MRD3, Span7	1.76	1.90	2.11	1.72	1.89	2.24
	MRD5, Span11	1.75	1.91	2.21	1.73	1.91	2.12
	MRD7, Span15	1.75	1.93	2.30	1.74	1.94	2.10
	MRD10, Span21	1.74	1.97	2.38	1.74	1.97	2.12
Axial Resolution	MRD3, Span7	2.99	3.43	5.67	2.98	3.49	5.60
	MRD5, Span11	3.05	3.50	5.66	3.04	3.48	5.63
	MRD7, Span15	3.10	3.55	5.75	3.09	3.53	5.62
	MRD10, Span21	3.14	3.58	5.93	3.08	3.57	5.82

MRD: Maximum Ring Difference, AFOV: Axial Field of View

in the SNR. To mitigate this reduction, the imaging duration and consequently the anesthesia time must be extended. Conversely, higher MRD and span values improve the SNR but can increase noise contributions from random events, which may ultimately compromise the quality of the reconstructed images.

High MRD and span values in image reconstruction, while improving SNR, introduce significant axial distortion and inter-slice activity misassignment, as demonstrated by uniform phantom study (Figures 4 & 5). This misassignment leads to activity overestimation, especially in regions of high activity gradients. The severity of this artifact increases with higher MRD and span and is exacerbated on scanners with larger axial fields of view, suggesting a relationship with system spatial encoding. Similar axial distortion and inter-slice activity misassignment, attributed to SSRB, were also observed in Defrise disk phantom studies in a clinical PET/CT scanner [14], a mini-Defrise phantom in small animal PET (A-PET) [31], and a grid of point sources [7].

Hasegawa et al. reported a span- and MRD-dependent degradation of axial resolution in their study, observing no effect of increased span at the scanner's center but significant deterioration at radial distances of 10 and 20 cm [13]. Brix et al. similarly observed a reduction in axial resolution as the span increased [4]. Conversely, our analysis revealed no significant impact of span or MRD on axial spatial resolution. This discrepancy may be attributable to the Xtrim-PET scanner's limited axial FOV, which inherently restricts the extent of axial data compression.

The RC and SOR remained largely unaffected by variations in span and MRD, suggesting that quantitative accuracy is robust to SSRB parameter changes. However, the introduction of artifacts in non-uniform regions underscores the need for advanced rebinning algorithms, such as multi-slice rebinning (MSRB) [7] or Fourier rebinning (FORE) [8], which may mitigate these distortions by leveraging more sophisticated data handling techniques.

In conclusion, our findings demonstrate that while higher span and MRD values improve SNR and image uniformity, they also introduce axial distortions and activity misassignment, particularly in regions with steep activity gradients. These trade-offs should be carefully considered when optimizing rebinning parameters for specific imaging applications. Future research should focus on integrating advanced rebinning algorithms and 3D reconstruction

techniques to address these challenges and further enhance the performance of preclinical PET imaging systems.

Conclusion

This work investigated the influence of MRD and span within the SSRB algorithm on both the image quality and accuracy of quantitative measurements of the preclinical Xtrim-PET scanner. While higher MRD and span values improve SNR and image uniformity, they introduce axial distortion and activity misassignment, particularly in regions with steep activity gradients, leading to an overestimation of activity concentration. However, increased span and MRD did not affect axial resolution, given the scanner's limited axial FOV. The observed axial distortion highlights the limitations of SSRB at high MRD and span.

Acknowledgment

The authors gratefully acknowledge the support of Parto Nagar Persia (PNP) Company.

Authors' Contribution

T. Zare and M. Ghorbanzadeh were involved in gathering the data and preparing and writing the original draft. T. Zare, M. Ghorbanzadeh, B. Teimourian Fard, P. Sheikhzadeh, S. Hariri Tabrizi, P. Ghafarian, and MH Farahani were involved in analyzing the data. MR. Ay and MH. Farahani conceived of the presented idea. All authors were involved in the design and implementation of the research. All authors read, modified, reviewed, and approved the final version of the manuscript.

Ethical Approval

This study was conducted under the ethical protocols of Tehran University of Medical Sciences (TUMS). No animal or human participants were involved in this study.

Funding

This work was supported through grant No. 55581 from the Tehran University of Medical Sciences.

Conflict of Interest

None

References

1. Miyaoka RS, Lehnert AL. Small animal PET: a review of what we have done and where we are going. *Phys Med Biol.* 2020;**65**(24):24TR04. doi: 10.1088/1361-6560/ab8f71. PubMed PMID: 32357344.
2. Efthimiou N, Wright JD, Clayton L, Renard I, Zagni F, Caribé PR, et al. Influence of multiple animal scanning on image quality for the sedecal superArgus2R preclinical PET scanner. *Frontiers in Physics.* 2021;**8**:531662. doi: 10.3389/fphy.2020.531662.
3. Zaidi H. Quantitative analysis in nuclear medicine imaging. Springer; 2006.
4. Brix G, Zaers J, Adam LE, Bellemann ME, Ostertag H, Trojan H, et al. Performance evaluation of a whole-body PET scanner using the NEMA protocol. National Electrical Manufacturers Association. *J Nucl Med.* 1997;**38**(10):1614-23. PubMed PMID: 9379202.
5. De Bernardi E, Mazzoli M, Zito F, Baselli G. Evaluation of frequency-distance relation validity for FORE optimization in 3-D PET. *IEEE Transactions on Nuclear Science.* 2007;**54**(5):1670-8. doi: 10.1109/TNS.2007.905175.
6. Daube-Witherspoon ME, Muehllehner G. Treatment of axial data in three-dimensional PET. *J Nucl Med.* 1987;**28**(11):1717-24. PubMed PMID: 3499493.
7. Lewittt RM, Muehllehner G, Karpt JS. Three-dimensional image reconstruction for PET by multi-slice rebinning and axial image filtering. *Phys Med Biol.* 1994;**39**(3):321-39. doi: 10.1088/0031-9155/39/3/002. PubMed PMID: 15551583.
8. Defrise M, Kinahan PE, Townsend DW, Michel C, Sibomana M, Newport DF. Exact and approximate rebinning algorithms for 3-D PET data. *IEEE Trans Med Imaging.* 1997;**16**(2):145-58. doi: 10.1109/42.563660. PubMed PMID: 9101324.
9. Liu X, Comtat C, Michel C, Kinahan P, Defrise M, Townsend D. Comparison of 3-D reconstruction with 3D-OSEM and with FORE+OSEM for PET. *IEEE Trans Med Imaging.* 2001;**20**(8):804-14. doi: 10.1109/42.938248. PubMed PMID: 11513031.
10. Bendriem B, Townsend DW. The theory and practice of 3D PET. Springer Science & Business Media; 1998.
11. Defrise M, Kinahan PE, Michel CJ. Image reconstruction algorithms in PET. In: Positron emission tomography: basic sciences. London: Springer; 2005. p. 63-91.
12. Fahey FH. Data acquisition in PET imaging. *J Nucl Med Technol.* 2002;**30**(2):39-49. PubMed PMID:

12055275.

13. Hasegawa T, Wada Y, Murayama H, Nakajima T. Basic performance of the PET scanner, EXACT HR/sup+/, with adjustable data-acquisition parameters. In: IEEE Nuclear Science Symposium Conference Record 1998 IEEE Nuclear Science Symposium and Medical Imaging Conference (Cat. No. 98CH36255); Toronto, ON, Canada: IEEE; 1998. p. 1721-8.
14. López-Montes A, Galve P, Udias JM, Cal-González J, Vaquero JJ, Desco M, Herraiz JL. Real-time 3D PET image with pseudoinverse reconstruction. *Appl Sci.* 2020;**10**(8):2829. doi: 10.3390/app10082829.
15. Tai YC, Ruangma A, Rowland D, Siegel S, Newport DF, Chow PL, Laforest R. Performance evaluation of the microPET focus: a third-generation microPET scanner dedicated to animal imaging. *J Nucl Med.* 2005;**46**(3):455-63. PubMed PMID: 15750159.
16. Mackewn JE, Lerche CW, Weissler B, Sunassee K, De Rosales RT, Phinikaridou A, et al. PET performance evaluation of a pre-clinical SiPM-based MR-compatible PET scanner. *IEEE Transactions on Nuclear Science.* 2015;**62**(3):784-90. doi: 10.1109/TNS.2015.2392560.
17. Angelis G, Bickell M, Kyme A, Ryder W, Zhou L, Nuyts J, et al. Calculated attenuation correction for awake small animal brain PET studies. In IEEE nuclear science symposium and medical imaging conference (2013 NSS/MIC); Seoul, Korea (South): IEEE; 2013. p. 1-4.
18. Popota FD, Aguiar P, Herance JR, Pareto D, Rojas S, Ros D, et al. Comparison of the performance evaluation of the MicroPET R4 scanner according to NEMA standards NU 4-2008 and NU 2-2001. *IEEE Transactions on Nuclear Science.* 2012;**59**(5):1879-86. doi: 10.1109/TNS.2012.2208760.
19. Amirrashedi M, Sarkar S, Ghafarian P, Hashemi Shahraki R, Geramifar P, Zaidi H, Ay MR. NEMA NU-4 2008 performance evaluation of Xtrim-PET: A prototype SiPM-based preclinical scanner. *Med Phys.* 2019;**46**(11):4816-25. doi: 10.1002/mp.13785. PubMed PMID: 31448421.
20. Sajedi S, Zeraatkar N, Taheri M, Kaviani S, Khanmohammadi H, Sarkar S, et al. Development and preliminary results of Xtrim-PET, a modular cost-effective preclinical scanner. *Nuclear Instruments and Methods in Physics Research Section A: Accelerators, Spectrometers, Detectors and Associated Equipment.* 2019;**940**:288-95. doi: 10.1016/j.nima.2019.06.009.
21. Jan S, Santin G, Strul D, Staelens S, Assié K, Autret D, et al. GATE: a simulation toolkit for PET and SPECT. *Phys Med Biol.* 2004;**49**(19):4543-61. doi: 10.1088/0031-9155/49/19/007. PubMed PMID: 15552416. PubMed PMCID: PMC3267383.
22. Sheikhzadeh P, Sabet H, Ghadiri H, Geramifar P, Mahani H, Ghafarian P, Ay MR. Development and validation of an accurate GATE model for NeuroPET scanner. *Phys Med.* 2017;**40**:59-65. doi: 10.1016/j.ejmp.2017.07.008. PubMed PMID: 28716541.
23. Zeraatkar N, Ay MR, Ghafarian P, Sarkar S, Geramifar P, Rahmim A. Monte Carlo-based evaluation of intercrystal scatter and penetration in the PET subsystem of three GE Discovery PET/CT scanners. *Nuclear Instruments and Methods in Physics Research Section A: Accelerators, Spectrometers, Detectors and Associated Equipment.* 2011;**659**(1):508-14. doi: 10.1016/j.nima.2011.07.049.
24. Pells S, Cullen DM, Deidda D, Denis-Bacelar AM, Fenwick A, Ferreira KM, et al. Quantitative validation of Monte Carlo SPECT simulation: application to a Mediso AnyScan GATE simulation. *EJNMMI Phys.* 2023;**10**(1):60. doi: 10.1186/s40658-023-00581-4. PubMed PMID: 37777689. PubMed PMCID: PMC10542438.
25. Bahadorzadeh B, Faghihi R, Sina S, Aghaz A, Rahmim A, Ay MR. Design and implementation of continuous bed motion (CBM) in Xtrim preclinical PET scanner for whole-body Imaging: MC simulation and experimental measurements. *Phys Med.* 2024;**123**:103395. doi: 10.1016/j.ejmp.2024.103395. PubMed PMID: 38843650.
26. NEMA. Performance Measurements of Small Animal Positron Emission Tomographs. NEMA Standards Publication NU 4-2008; Rosslyn: National Electrical Manufacturers Association; 2008.
27. Chang LT. A method for attenuation correction in radionuclide computed tomography. *IEEE Transactions on Nuclear Science.* 1978;**25**(1):638-43. doi: 10.1109/TNS.1978.4329385.
28. Loening AM, Gambhir SS. AMIDE: a free software tool for multimodality medical image analysis. *Mol Imaging.* 2003;**2**(3):131-7. doi: 10.1162/15353500200303133. PubMed PMID: 14649056.
29. Zanzonico P. Routine quality control of clinical nuclear medicine instrumentation: a brief review. *J Nucl Med.* 2008;**49**(7):1114-31. doi: 10.2967/jnumed.107.050203. PubMed PMID: 18587088. PubMed PMCID: PMC2703015.
30. Adam LE, Zaers J, Ostertag H, Trojan H, Bellemann ME, Brix G, Lorenz WJ. Performance evaluation of the whole-body PET scanner ECAT EXACT HR/sup+. In IEEE Nuclear Science Symposium Conference Record; Anaheim, CA, USA: IEEE; 1996. p. 1270-4.
31. Daube-Witherspoon ME, Popescu LM, Matej S, Cardi CA, Lewitt RM, Karp JS. Rebinning and reconstruction of point source transmission data for positron emission tomography. In IEEE Nuclear Science Symposium Conference Record (IEEE Cat. No.03CH37515); Portland, OR, USA: IEEE; 2003. p. 2839-43.